

X-ray observations of low-power FR I radio galaxies

E. Trussoni¹, F. Vagnetti², S. Massaglia³, L. Feretti⁴, P. Parma⁴, R. Morganti⁴, R. Fanti^{4,5}, and P. Padovani^{2,6,*}

¹ Osservatorio Astronomico di Torino, Strada dell'Osservatorio 20, I-10025 Pino Torinese (TO), Italy

² Dipartimento di Fisica, Università di Roma "Tor Vergata", Via della Ricerca Scientifica, I-00133 Roma, Italy

³ Dipartimento di Fisica Generale dell'Università, Via P. Giuria 1, I-10125 Torino, Italy

⁴ Istituto di Radioastronomia del CNR, Via Gobetti 101, I-40129 Bologna, Italy

⁵ Dipartimento di Fisica dell'Università, Via Irnerio 46, I-40126 Bologna, Italy

⁶ Space Telescope Science Institute, 3700 San Martin Drive, Baltimore, MD 21218, USA

Received 12 March 1999 / Accepted 16 June 1999

Abstract. According to unified schemes for Active Galactic Nuclei, low-power, Fanaroff-Riley type I (FR I), radio galaxies are thought to be BL Lacs with their jets pointing at relatively large angles with respect to the line of sight. X-ray observations of FR I sources can test this scenario and constrain the presence of obscuring material around the nucleus. In this paper we discuss the X-ray properties of three FR I radio galaxies 3C 78, OH-342 and PKS 0620-52, observed with the BeppoSAX satellite in the 0.2–10 keV energy range. The narrow-field instruments on board BeppoSAX have detected extended thermal X-ray emission from a hot galactic corona (3C 78) and intra-cluster gas (OH-342 and PKS 0620-52). However, a detailed spectral analysis suggests that a non-thermal (likely nuclear) component can also significantly contribute to the total flux, especially in the case of 3C 78 and OH-342. This emission from the central region appears basically unabsorbed, in agreement with observations in other bands. The X-ray spectral luminosity of the nucleus of these three objects is correlated with the radio core luminosity, consistently with previous data on other FR I radio galaxies.

Key words: galaxies: active – galaxies: individual: 3C 78; OH-342; PK0620-52 – galaxies: nuclei

1. Introduction

Radio galaxies play a relevant role in unified schemes for Active Galactic Nuclei (AGN; see e.g., Urry & Padovani 1995). High-power radio galaxies (Fanaroff-Riley II, FR II; Fanaroff & Riley 1974) are considered to be the parent population of radio loud quasars, while low-power radio galaxies (Fanaroff-Riley I, FR I) are associated to BL Lac objects. The unification of quasars with FR II radio galaxies requires obscuration of infrared through ultraviolet light by optically thick gas and dust and relativistic beaming of radio jets. The weakness of the X-ray continuum from FR II radio galaxies relative to quasars is

also consistent with the idea of an obscured nucleus. In Cygnus A the variability of the X-ray emission argues for a compact nuclear source (Arnaud et al. 1987) and the X-ray spectrum is commensurated with a high column density of cold gas along the line of sight (Ward et al. 1991, Ueno et al. 1994).

The unification of BL Lac objects with FR I radio galaxies also requires relativistic beaming, while the presence of an absorbing torus in such objects is still an open question. This possibility is supported by the lack in FR I of broad lines that are conversely present in some BL Lacs (e.g., Vermeulen et al. 1995, Corbett et al. 1996). On the other hand, very recent results from HST show that circumnuclear dust lanes are commonly present in low-luminosity radio galaxies, but the nuclei appear basically not obscured (De Koff et al. 1996, Chiaberge et al. 1999).

As far as the X-ray emission is concerned, a relatively weak nuclear component is expected in FR Is if, according to unified scheme, the relativistic jet is misdirected with respect to the line of sight. The X-ray emission could be further reduced in the soft band by an obscuring torus.

Detection of non-thermal X-ray emission in FR Is, however, is complicated by the fact that the parent galaxies have hot coronae (temperature ≈ 1 keV; Fabbiano 1989) and often are members of groups or clusters embedded in large clouds of hot plasmas (temperature $\approx 2-8$ keV; Sarazin 1986). Therefore, even though several FR I sources have been detected in the *Einstein* Extended Medium Sensitivity Survey (EMSS) and in the ROSAT All Sky Survey (RASS), it is difficult to separate any contribution of the active nucleus from the extended emission.

Worrall & Birkinshaw (1994) have observed a small sample of FR I radio galaxies with the ROSAT PSPC. Their data analysis points out an apparently pointlike, power-law emission, possibly correlated with the core radio power, in addition to the thermal extended flux (emitted from the hot galactic halo). The total luminosities of these two spectral components are comparable ($\sim 10^{42-43}$ erg s⁻¹), although it is not clear whether the non-thermal emission originates in the very central region or at some distance along the jet (Worrall 1997).

More information on these objects can be obtained from observations at harder X-ray energies. In this case, in fact, a non-thermal nuclear component could be more easily detected, and

Send offprint requests to: E. Trussoni (Torino)

* Affiliated to the Astrophysics Division, Space Science Department, European Space Agency

any nuclear absorption would enhance the evidence in favour of a non-thermal contribution. We present the results of BeppoSAX observations (in the 0.2–10 keV energy band) of three low brightness radio galaxies: 3C 78, OH–342 and PKS 0620–52, and discuss them in the framework of the unified scheme for FR I and BL Lac objects. We will see that, even considering the presence of the thermal emission from the extended gas surrounding the galaxies (3C 78 is isolated, while the other two belong to small clusters), a non-thermal component is also very likely to be present.

The main properties of the sources at different wavelengths and previous X-ray data are summarized in Sect. 2, while the details of the present observations are given in Sect. 3. The results of the spectroscopic analysis are reported in Sect. 4. The discussion of the results and the astrophysical implications are in Sect. 5.

2. The sources

The basic, multi-wavelength observational properties of the three targets are given in Table 1 and presented in detail in the following ($H_0 = 50 \text{ km s}^{-1} \text{ Mpc}^{-1}$ is assumed throughout).

3C 78 (NGC 1218, PKS 0305+03). The radio galaxy 3C 78 is an isolated source associated with the S0 galaxy NGC 1218 at distance $D = 173 \text{ Mpc}$ with $B_{T_0} = 13.16$, corresponding to $M_{B_{T_0}} = -23.03$. An optical jet has been recently detected by the HST, with an extent of $\approx 1.4''$ ($\approx 1 \text{ kpc}$) at position angle $\approx 55^\circ$ (Sparks et al. 1995). This optical jet is almost coincident with a radio one-sided jet (Unger et al. 1984, Saikia et al. 1986). The IRAS satellite has detected infrared emission from NGC 1218 at 25μ ($\approx 110 \text{ mJy}$) and 100μ ($\approx 420 \text{ mJy}$; Knapp et al. 1990). The radio emission is characterized by a prominent nucleus, weak jets and diffuse structures (see Fig. 1). The low-brightness diffuse emission, observed at low resolution by Baum et al. (1988), has an extension of about $4'$, corresponding to a linear size of $\sim 200 \text{ kpc}$.

Few data have been collected on this source at X-ray energies, so far. In the *Einstein* IPC (0.2–4.0 keV) the source, not listed as an extended target, has a luminosity $9.4 \times 10^{42} \text{ erg s}^{-1}$, if a thermal spectrum with $T = 5 \text{ keV}$ is assumed (Fabbiano et al. 1992). Siebert et al. (1996), from RASS data, inferred an X-ray luminosity $1.9 \times 10^{43} \text{ erg s}^{-1}$ (0.1–2.4 keV), assuming a power-law spectrum with photon index $\alpha = 1.9$.

OH–342 (PKS 0625–35). This source is a cD elliptical galaxy at distance $D = 329 \text{ Mpc}$, and is the first ranked member of the cluster A 3392, which is poor and classified of richness 1 (Abell et al. 1989). The optical image and radio maps are presented in Fig. 2. The radio emission is dominated by the bright core, with a one-sided jet oriented to SE. A low-brightness extended radio halo is visible in the lower resolution map of Ekers et al. (1989), with a total extent of $\sim 4'$, corresponding to a linear size of $\sim 340 \text{ kpc}$.

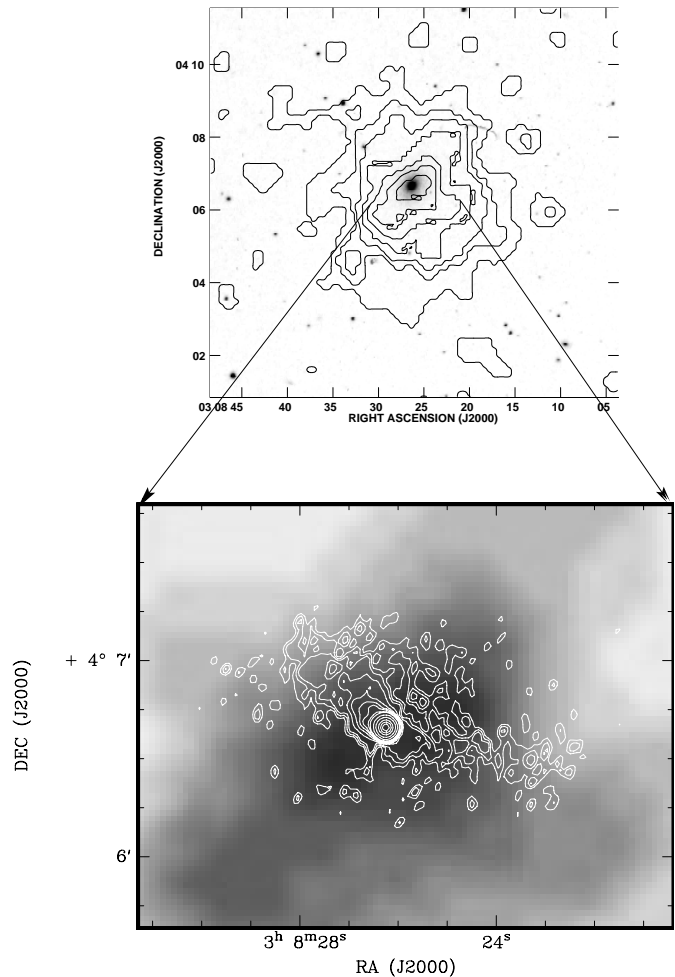


Fig. 1. *Top:* Overlay of the MECS X-ray contours (1–10 keV) onto the grey-scale image of the optical red image taken from the Digitized Palomar Sky Survey (PSS) of 3C 78. The X-ray map has been smoothed to a Gaussian with $28''$ (FWHM). Contours are at 20, 29, 41, 57, 74 and 90% of the peak ($0.19 \text{ cts arcsec}^{-2}$). *Bottom:* Overlay of the radio contour map onto the grey scale MECS image. The radio image was obtained with the VLA at 4.8 GHz (Morganti et al. 1993) with resolution $3.9'' \times 3.5''$ (p.a. -31°). Contour levels are at 0.5, 0.75, 1, 1.5, 2, 2.5, 3, 4, 5, 10, 20, 40, 60, 80% of the peak ($=0.844 \text{ Jy/beam}$).

The only X-ray data on this source, available so far, are from the RASS. Siebert et al. (1996) (see also Ebeling et al. 1996) deduced a luminosity $1.3 \times 10^{44} \text{ erg s}^{-1}$ (assuming a power-law spectrum with $\alpha = 1.9$), from an apparently extended X-ray emission.

PKS 0620–52. Few details are available on the galaxy associated with this target, which is the brightest member of a cluster at distance $D = 309 \text{ Mpc}$. Some spectroscopic features of this object are typical of early-type galaxies (Tadhunter et al. 1993). In the radio band the source appears as an asymmetric, head-tail radio galaxy, with a short eastern tail, and the western tail of size $\sim 1'$ (see Fig. 3). More extended low-brightness radio tails can be seen in the lower resolution image of Jones & McAdam

Table 1. Basic properties of the observed sources

Source	RA (J2000)	DEC (J2000)	z	m_V	Galaxy	Envir.	P_c^a	P_{tot}^a	P_{CN}^b
3C 78	03 08 26.2	+04 06 39	0.029	13.8	S0	Isol.	0.36	1.3	6.4
OH-342	06 27 04.4	-35 28 54	0.055	16.5	cD	A 3392	0.81	2.9	15.0
PKS 0620-52	06 21 43.2	-52 41 36	0.051	15.5	E (?)	Cluster ^c	0.31	1.5	3.5

^a core and total radio luminosity $\times 10^{32} \text{ erg cm}^{-2} \text{ s}^{-1} \text{ Hz}^{-1}$ at 5 GHz (Morganti et al. 1997)

^b ratio, at 1.4 GHz, of P_c to P_{cm} , the median value of P_c (see Sect. 5)

^c EMSS name: MS0620.6-5239

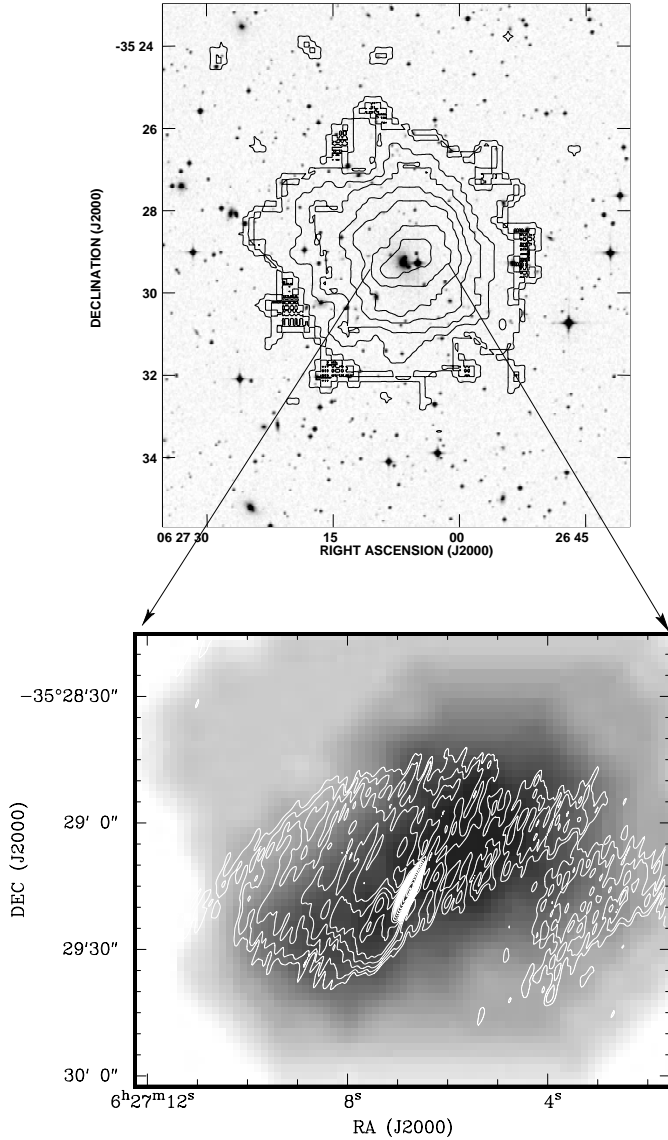


Fig. 2. *Top:* Overlay of the MECS X-ray contours (1–10 keV) onto the grey-scale image of the optical PSS image of OH-342. The X-ray map has been smoothed to a Gaussian of 28'' (FWHM). Contours are at 10, 18, 26, 39, 52, 65 and 78% of the peak (0.27 cts arcsec⁻²). *Bottom:* Overlay of the radio contour map onto the grey scale MECS image. The radio image was obtained with the VLA at 4.8 GHz (Simpson 1994) with resolution 5.25'' \times 1.15'' (p.a. -25°). Contour levels are at 0.2, 0.5, 0.75, 1, 1.5, 2, 2.5, 3, 4, 5, 10, 20, 40, 60, 80% of the peak (=1.12 Jy/beam).

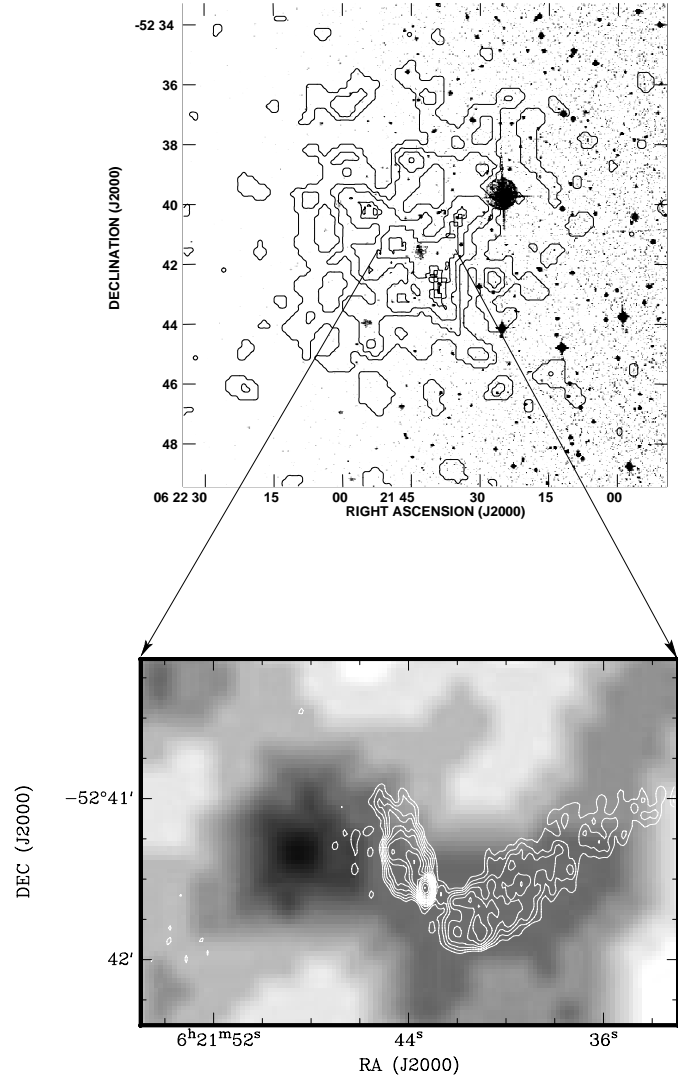


Fig. 3. *Top:* Overlay of the MECS X-ray contours (1–10 keV) onto the grey-scale optical PSS image of PKS 0620-52. The X-ray map has been smoothed to a Gaussian with 28'' (FWHM). In the left half of the optical plate the obscuring light of Canopus has been subtracted. Contours are at 18, 30, 42, 61 and 85% of the peak (0.13 cts arcsec⁻²). *Bottom:* Overlay of the radio contour map onto the grey scale MECS image. The radio image was obtained with the ATCA at 5 GHz (Morganti et al. 1993) with resolution 4.7'' \times 2.7'' (p.a. 2°). Contour levels are at 0.5, 0.75, 1, 1.5, 2, 2.5, 3, 4, 5, 10, 20, 40, 60, 80% of the peak (=0.262 Jy/beam).

(1992). They are similar in extent, each with a size of $\sim 3.5'$, corresponding to ~ 280 kpc.

In the EMSS (Gioia et al. 1984, Gioia & Luppino 1994) the source appears extended (size $\approx 10'$, EMSS catalogue number MS0620.6–5239), with a luminosity 2.0×10^{43} erg s $^{-1}$, if a non-thermal spectrum with $\alpha = 1.4$ is assumed. Also in the RASS PKS 0620–52 shows up as an extended source with a luminosity 4.1×10^{43} erg s $^{-1}$, assuming now a non-thermal emission with $\alpha = 1.9$ (Siebert et al. 1996).

3. Observations and data analysis

The details of our BeppoSAX observations are reported in Table 2. We remind the reader that this mission covers the 0.1–300 keV energy range with different instruments. We have employed the three Medium Energy Concentrator Spectrometers (MECS, 1.5–10 keV) and the Low Energy Concentrator Spectrometers (LECS, 0.1–10 keV) with imaging capabilities (spatial resolution of $\approx 2'$, FWHM). No source signal was detected in the high energy detectors: the High Pressure Gas Scintillation Proportional Counter (HPGSPC) and the Phoswich Detector System (PDS). A description of the satellite payload is given in Boella et al. (1997a, 1997b), Parmar et al. (1997), Manzo et al. (1997) and Frontera et al. (1997).

The event files from both instruments have been obtained by processing the original raw data through the packages FTOOLS (ver. 3.5) and SAXDAS (ver. 1.3.0). The adopted matrices for the effective areas and the instrumental response were those released in September 1997. The choice of the extraction radius, r_{extr} , depends on the radial distribution of the counts. Furthermore, the vignetting effect should be taken into account for sources with size $> 4'$. We have seen that in the MECS $\approx 90\%$ of the source photons (at 1σ uncertainty) are within $4'$ for 3C 78 and within $6'$ for the other two targets. Then, from the calibration data (Fiore et al. 1999) we have estimated that, with this extraction radius, the underestimate of the count rate due to the vignetting is $< 15\%$ of the total counts for PKS 0620–53 and $< 7\%$ for OH–342.

The LECS extraction radius for point sources is generally taken to be larger than the MECS one, due to the different point spread functions. In our case, however, in order to reduce the vignetting effect and given the relatively low LECS count rate (mainly for 3C 78 and PKS 0620–52), we have chosen a somewhat smaller value of r_{extr} for the LECS (the underestimate of the count rate is negligible). Therefore, we have assumed for both instruments $r_{\text{extr}} = 4'$ for 3C 78 and $r_{\text{extr}} = 6'$ for OH–342 and PKS 0620–52. The counts for each source are reported in Table 2.

The background has been extracted by merging different exposures of flat fields with the same r_{extr} of the target region (the observations of the three MECS have been merged together). We have checked for both instruments that the background flux, detected in regions far from the source, is consistent (within statistical errors) with the flux detected from the same regions in the flat field exposures.

We have used the XIMAGE package (ver. 2.53) for imaging, and the XSPEC package (ver. 9.0) for the spectral analysis. The events have been rebinned such that each new bin contains at least 20 counts. We have adopted the Mekal model (Kaastra 1992) to fit thermal emission from an optically thin plasma, including, for the MECS data analysis, the energy channels 37–220 (≈ 1.5 –9.5 keV), and the energy channels 10–700 (≈ 0.2 –5 keV) for the LECS. The spectral fits have been performed for the two instruments simultaneously, letting the LECS/MECS normalization f free to vary, due to uncertainties in the LECS calibration (the expected values are $0.65 \lesssim f \lesssim 0.85$, Fiore et al. 1999).

To estimate f we proceeded as follows: we first evaluated f with its 1σ fluctuations from a preliminary fit, then f was fixed to its more likely value if this was within $0.65 \leq f \pm \sigma \leq 0.85$. For $f \pm \sigma$ outside this interval we have assumed $f + \sigma$ for $f < 0.65$ and $f - \sigma$ for $f > 0.85$. Notice that, due to the low count rates, useful results were obtained only with some spectral parameters kept fixed. The assumptions made will be discussed and commented in detail for each target. The errors reported in the text and in the tables are the 68% uncertainties (1σ) for one interesting parameter ($\Delta \chi^2 = 1$).

4. Results

The MECS X-ray images of OH–342 and PKS 0620–52 are clearly extended with respect to the point spread function, with a total size of $\approx 8'$ and $\approx 10'$, respectively. The brightness profile of 3C 78 is basically consistent with a pointlike source, even though an excess is very likely to be present at radii $\gtrsim 2'$ from the center. This is expected, considering that the sources are embedded in the coronal or intracluster gas. The peak of the X-ray emission in the MECS coincides (within the errors) with the positions of the three radio galaxies: the brightness distribution is more peaked for 3C78 and OH–342, while it is flatter for PKS 0620–52. Furthermore, we notice that the X-ray region appears wider than the extent of the radio structures, also considering the presence of low brightness extended emission. Overlays of X-ray (MECS), optical and radio maps are reported in Figs. 1–3. The limited spatial resolution of the instrument does not allow a detailed analysis of the X-ray brightness distribution.

4.1. Spectral analysis: one-component model

As discussed above, we expect most of the X-ray emission to be of thermal origin, with a possible contribution from a nuclear, power-law component. In the data analysis, we have adopted the following general procedure: we have first fitted the data to a single thermal model, leaving at first all the parameters free, and the results are reported in Table 3. In order to obtain a better fit, we have then fixed the hydrogen absorption (to the galactic value) and the metallicity \mathcal{M} (with respect to the standard cosmic abundances). These spectral fits are shown in Figs. 4a,b,c with the fit parameters again in Table 3. The reasonable values found for metallicity are $\mathcal{M} = 0.5$ in galactic coronae (3C 78)

Table 2. Observational details

Source	Obs. date	$t_{\text{exp,MECS}}$	$t_{\text{exp,LECS}}$	Net counts ^{a,b} _{MECS}	Net counts ^b _{LECS}
3C 78	7/1/1997	20594 s	8890 s	521 ± 28	143 ± 25
OH-342	5/10/1996	17528 s	8211 s	1805 ± 47	568 ± 32
PKS 0620-52	2-3/12/1996	13689 s	4458 s	618 ± 31	123 ± 24

^a merging the counts of the three instruments

^b Source - background $\pm 1\sigma$; $r_{\text{extr}} = 4'$ (3C 78) and $r_{\text{extr}} = 6'$ (OH-342 and PKS 0620-52)

Table 3. Fits with a thermal spectrum (parameters without errors have been fixed)

Source	f	N_{H}^{a}	T (keV)	\mathcal{M}	A_{th}^{b} ($\times 10^{-3} \text{ cm}^{-5}$)	χ_{red}^2 (d.o.f.)
3C 78	0.70	$2.6^{+3.0}_{-1.6}$	$2.75^{+0.45}_{-0.32}$	$0.30^{+0.30}_{-0.23}$	$1.93^{+0.32}_{-0.25}$	1.47 (31)
		7.3	$2.54^{+0.30}_{-0.25}$	0.5	$1.92^{+0.15}_{-0.16}$	1.45 (33)
OH-342	0.87	$4.3^{+1.1}_{-0.8}$	$2.82^{+0.18}_{-0.16}$	$0.27^{+0.12}_{-0.11}$	$7.97^{+0.51}_{-0.47}$	1.21 (90)
		7.1	$2.67^{+0.15}_{-0.13}$	0.3	$8.30^{+0.36}_{-0.37}$	1.24 (92)
PKS 0620-52	0.70	$4.6^{+4.5}_{-2.3}$	$2.62^{+0.38}_{-0.29}$	$0.14^{+0.39}_{-0.14}$	$4.07^{+0.61}_{-0.50}$	0.69 (35)
		5.2	$2.53^{+0.27}_{-0.23}$	0.3	$3.88^{+0.34}_{-0.33}$	0.67 (37)

^a $\times 10^{20} \text{ cm}^{-2}$ (when fixed, $N_{\text{H}} \equiv N_{\text{H,gal}}$)

^b $A_{\text{th}} = 10^{-14} / (4\pi D^2) \int n_{\text{e}} n_{\text{H}} dV$, D is the source distance, and n_{e} , n_{H} the electronic and hydrogen densities

Table 4. Fits with a two-component spectrum (quantities without errors have been fixed)

Source	$N_{\text{H,loc}}^{\text{a}}$	f	α	T (keV)	χ_{red}^2	$L_{\text{X,th,m}}^{\text{b}}$	$L_{\text{X,pl,m}}^{\text{b}}$	$L_{\text{X,th,s}}^{\text{c}}$	$L_{\text{X,pl,s}}^{\text{c}}$
3C 78 ^d	0	0.65	1.7	$1.39^{+0.23}_{-0.21}$	1.09	0.30	0.39	0.55	0.31
			2.3	$0.96^{+0.60}_{-0.21}$	1.05	0.06	0.60	0.19	1.5
	1	0.70	1.7	$2.08^{+0.23}_{-0.18}$	1.08	0.65	1.73	0.87	1.39
			2.3	$2.05^{+0.22}_{-0.18}$	1.08	0.65	3.06	0.88	7.54
OH-342 ^d	0	0.77	1.7	$1.63^{+0.13}_{-0.11}$	1.00	5.0	4.3	8.8	3.5
			2.3	$1.70^{+0.31}_{-0.26}$	0.95	2.0	7.1	3.4	17
	1	0.81	1.7	$2.27^{+0.12}_{-0.11}$	1.05	8.2	14.4	11.0	12.7
			2.3	$2.24^{+0.12}_{-0.11}$	1.05	8.2	25.0	11.1	61.9
PKS 0620-52 ^d	0	0.70	1.7	$1.86^{+0.41}_{-0.29}$	0.60	2.2	1.2	3.5	1.0
			2.3	$2.38^{+0.36}_{-0.38}$	0.65	2.3	1.1	2.9	2.7
	1	0.70	1.7	$2.44^{+0.32}_{-0.25}$	0.66	3.2	3.1	4.0	1.9
			2.3	$2.44^{+0.33}_{-0.26}$	0.66	3.2	2.4	4.0	7.8

^a $\times 10^{24} \text{ cm}^{-2}$

^b $\times 10^{43} \text{ erg s}^{-1}$; medium energy band: 1–10 keV

^c $\times 10^{43} \text{ erg s}^{-1}$; soft energy band: 0.1–2.4 keV

^d $N_{\text{H}} \equiv N_{\text{H,gal}}$, $\mathcal{M} = 0.5$ (3C 78) and $\mathcal{M} = 0.3$ (OH-342 and PKS 0620-52).

and $\mathcal{M} = 0.3$ in clusters (OH-342 and PKS 0620-52; see e.g., Feretti et al. 1995, Massaglia et al. 1996, Trussoni et al. 1997).

3C 78. The fit with a single thermal spectrum with all free parameters is poor. The value of the column density has large uncertainty, and its upper limit is close to $N_{\text{H,gal}}$, while the metallicity is basically consistent with the expected value. The quality of the fit does not change by fixing N_{H} and \mathcal{M} . A count excess is evident in the spectrum at high energies ($\gtrsim 5$ keV), above the possible iron line at ≈ 6.5 keV (see Fig. 4a).

OH-342. The spectral features are similar to the previous case but the single thermal spectrum appears now to fit the data better. The column density is better constrained, with its upper value close to $N_{\text{H,gal}}$ and the metallicity in the expected range. In Fig. 4b we notice again the excess of photons at energies higher than the energy of the Fe line. A soft excess is also present at ≈ 0.3 – 0.8 keV.

PKS 0620-52. The low flux ($\approx 1/3$ of OH-342, distributed on a comparable area) yields a larger uncertainty on the parameters (see Table 3, Fig. 4c).

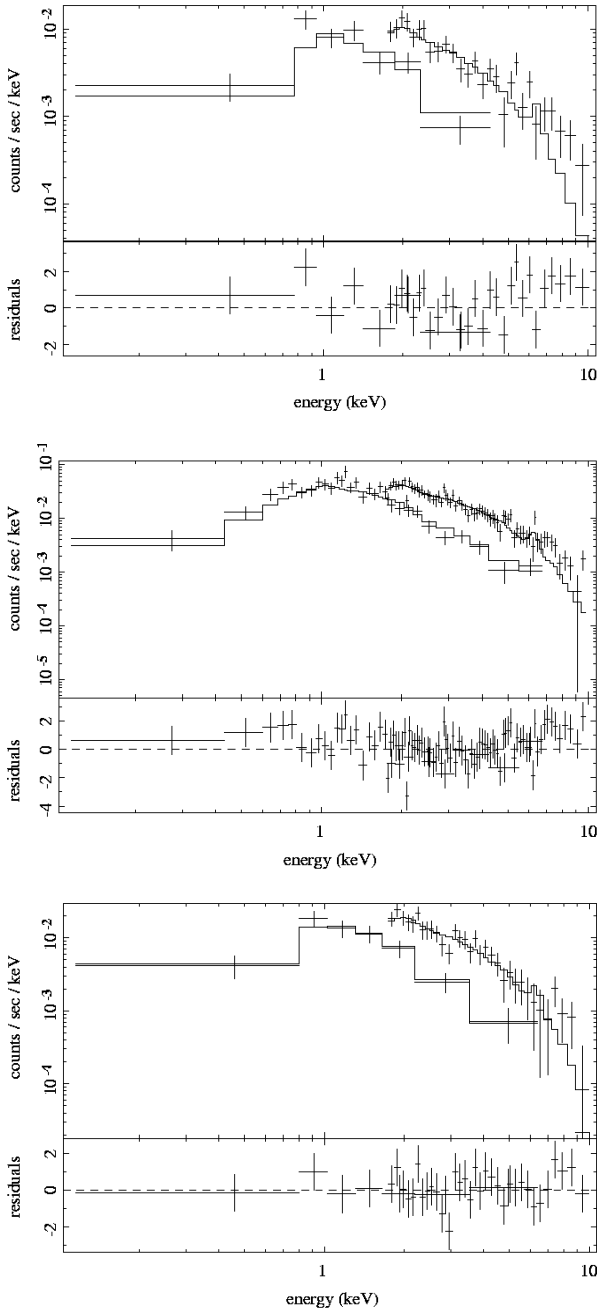


Fig. 4. X-ray spectrum of 3C 78 (*upper panel*), OH-342 (*middle panel*) and PKS 0620-52 (*lower panel*) fitted to a thermal model. We have fixed $N_{\text{H}} \equiv N_{\text{H,gal}}$ for all the targets, and $\mathcal{M} = 0.5$ (3C 78) and $\mathcal{M} = 0.3$ (OH-342 and PKS 0620-52).

4.2. Spectral analysis: two-component model

The excess at high energies with respect to the thermal spectrum, found for the sources and discussed in the above subsection, suggests the existence of a second, harder, component possibly related to the nuclear source. We have therefore performed fits with a two-component model, i.e., a non-thermal component in addition to the thermal one. The fits with two spectra require ‘a priori’ assumptions on some spectral parameters to obtain good constraints on the remaining free parameters. By fixing only the

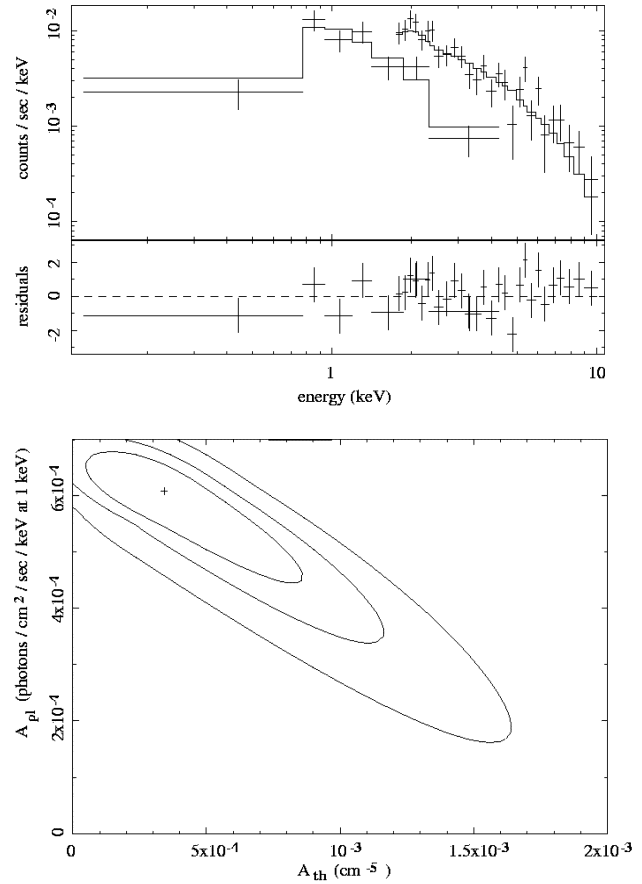


Fig. 5. Thermal + power-law X-ray spectrum (*upper panel*) and confidence contours of the normalization amplitudes of the two spectral components A_{th} and A_{pl} (*lower panel*) for 3C 78. We have assumed $N_{\text{H}} = N_{\text{H,gal}}$, $\mathcal{M} = 0.5$, $\alpha = 2.3$ and $N_{\text{H,loc}} = 0$.

value of N_{H} and of the metallicity in the thermal component (as in the single spectrum fit), the power-law photon index was still affected by very large uncertainties. We then had to fix its value, α , as well. As a guideline, we notice that the X-ray spectra of BL Lacs range between the values typical of High Energy Peaked BL Lacs (HBL, $\alpha \approx 2.5$) to those of Low Energy Peaked BL Lacs (LBL, $\alpha \approx 2.1$; Padovani & Giommi 1996, Padovani 1999). For FR I radio galaxies the available X-ray data yield much more uncertain values. Worrall & Birkinshaw (1994) (see also Capetti et al. in preparation) found $\alpha \sim 1.4$ (NGC 6251), $\alpha \sim 1.7$ (NGC 4261) and $\alpha \sim 2.4$ (3C 264). We have therefore considered both the possibilities of a flat and a steep spectrum, assuming for the photon index of the non-thermal component $\alpha = 1.7$ and $\alpha = 2.3$.

We have also taken into account the possible presence of obscuring material, by assuming a local absorption for the power-law spectrum up to $N_{\text{H,loc}} \sim 10^{24} \text{ cm}^{-2}$. Thus the remaining free parameters, obtained by the fitting procedure, are the normalization factors of the two spectra, A_{th} (cm^{-5}) and A_{pl} ($\text{photons cm}^{-2} \text{ s}^{-1} \text{ keV}^{-1}$ at 1 keV), and the temperature of the thermal plasma.

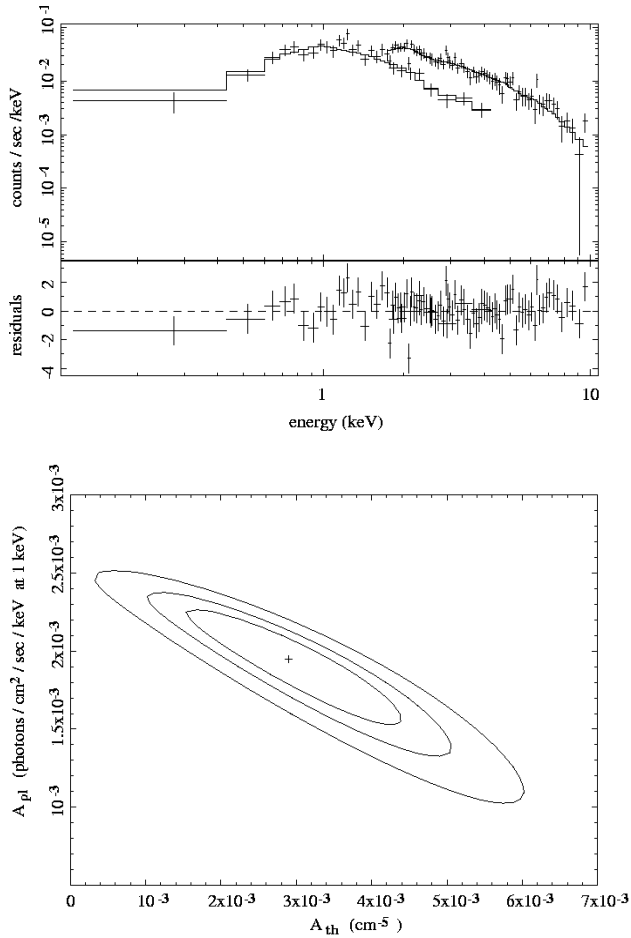


Fig. 6. The same as Fig. 5 for OH-342, assuming $\mathcal{M} = 0.3$.

The results are reported in Table 4 and Figs. 5–7. Employing an F -test, we have checked that the fits with the two-component spectra (with $N_{\text{H,loc}} = 0$) are improved, with respect to the case with the single spectrum, at a confidence level $> 99\%$ for OH-342 and 3C 78, while no conclusion can be drawn for PKS 0620–52 (improvement at a confidence level $\gtrsim 70\%$). Consistently, we see in Figs. 5 and 6 that for 3C 78 and OH-342 the presence of a power-law spectrum is likely at a level $> 3\sigma$, even though with quite large statistical uncertainties. In particular for 3C 78 the parameters of the thermal component are poorly defined for a steep, unabsorbed power-law spectrum (see Figs. 5). More uncertain is the case of PKS 0620–52 where we can claim the existence of a non-thermal component only at a confidence level $\gtrsim 1\sigma$, if its slope is quite flat and some local absorption is included (see Fig. 7).

The following general properties of the spectra can thus be deduced (see Table 4):

- 1) The values for the gas temperature are significantly lowered by the contribution of the power-law component with respect to the single thermal spectrum.
- 2) The relative contribution of the two components to the total flux depends on the slope of the power-law spectrum: $L_{\text{X,th}}$ increases with the steepness of the non-thermal component. Con-

versely, the temperature of the gas is not significantly affected by the value of the photon index α .

- 3) The spectral parameters are not critically affected by local absorption for $N_{\text{H,loc}} \lesssim 10^{24} \text{ cm}^{-2}$. For higher column densities both the gas temperature and the nuclear luminosity increase in the fits.

5. Discussion and conclusions

We have seen that the BeppoSAX spectral data are more consistent with a two-component model (thermal plus non-thermal) than with a single component (thermal) model, especially for 3C 78 and OH-342 (although with some residual uncertainties on the physical quantities). Additional information, needed to constrain the spectral parameters, can be obtained from the general X-ray properties of galaxies and clusters.

The typical temperatures of hot halos in early type galaxies are $\approx 0.5 - 1.5 \text{ keV}$. In addition a correlation has been found between optical and X-ray luminosities (see e.g. Forman et al. 1985, 1994, Donnelly et al. 1990, Trussoni et al. 1997). If we apply this correlation to 3C 78, the value of M_{BT_0} of the parent galaxy NGC 1218 would correspond to a luminosity in the ROSAT band $L_{\text{X}} = 2.3 \times 10^{42} \text{ erg s}^{-1}$. Our fits with a single thermal component disagree with these values, since they give a too high temperature and a luminosity ≈ 3 times higher ($L_{\text{X,th,s}} \approx 7 \times 10^{42} \text{ erg s}^{-1}$). The addition of a non-thermal component in the spectral model, yields more consistent values of T , and fits the hard photon excess. We notice also that, for an almost unabsorbed nucleus ($N_{\text{H,loc}} \approx 0$) and not too flat spectra ($\alpha \gtrsim 2$), the thermal luminosity component is consistent with the relation $L_{\text{X}} - L_{\text{B}}$ (see $L_{\text{X,th,s}}$ in Table 4). In Fig. 5 we plot the fitted spectrum and the confidence levels for the normalizations of the two spectral components. This last plot (lower panel) shows that a larger contribution to the total energy flux originates from the non-thermal nuclear component.

In OH-342, the comparison of our results with the $L_{\text{X}} - T$ correlation for clusters and Hickson compact groups (Ponman et al. 1996a,b) yields no stringent constraints on the parameters. The values of T and $L_{\text{X,th,s}}$, obtained from the fits with a single thermal model, are consistent with this relation (in the region of low brightness clusters). If a power-law component is added, the data still agree with the correlation, but are shifted to lower luminosities and temperatures, close to the boundary for compact groups (for which the $L_{\text{X}} - T$ relation is steeper). A large local nuclear absorption would enhance the luminosity to values considerably higher than expected for a cluster: we thus argue that even in this case the local column density is not large (we recall that the values of the thermal luminosities should be considered as lower limits, see Sect. 2). In any case, the quite large scatter of the data around the $L_{\text{X}} - T$ relation and the lack of detailed optical information on the cluster associated with OH-342 do not allow to say something more on the physical conditions and radiation processes. Finally, we note that both high and soft energy excesses can be fitted with $N_{\text{H,loc}} \approx 0$ and a quite steep ($\alpha > 2$) non-thermal component only (see Figs. 4 and 6).

The same arguments, although more uncertain, hold for PKS 0620–52 as well. In fact, very few optical data are available on the structure of this cluster, strongly contaminated by the light of Canopus. The thermal luminosities are basically consistent with the $L_X - T$ relation either for a single thermal spectrum or for a two-component model. However, a better agreement with this relation can be obtained by introducing some amount of local absorption and assuming a moderately flat spectrum (see Fig. 7).

Our data do not prove the presence of a nuclear X-ray component in our sources. We have seen, however, that there are reasonable, albeit indirect, clues in favor of this, especially for 3C 78 and OH–342. This view is further supported by radio observations. The ratio R between the core (P_c) and the extended radio power (P_e) is generally considered as an indicator of orientation of the nuclear jet. However, in view of the existing correlation between core and extended luminosity (De Ruiter et al. 1990), very likely intrinsic, it is definitely more preferable to use, as orientation indicator, the parameter P_{CN} . This parameter is defined as the ratio of the core luminosity of the source to the median value, P_{cm} , of core luminosities of sources with the same extended radio power, as expected from the correlation between P_c and P_e . We calculate $P_{CN} = R/R_m$ at 1.4 GHz, where R_m is the median value of R at a given extended luminosity, obtained from the relation given by De Ruiter et al. (1990):

$$\log R_m = 0.55 \log P_e + 11.76. \quad (1)$$

In presence of relativistic beaming effects, we expect that $P_{CN} >$ or $<$ 1 occurs in sources with angle between jet axis and line of sight $<$ or $>$ 60° , respectively. As reported in Table 1, in our sources we have $P_{CN} > 3.5$. This strongly suggests orientation angles $< 60^\circ$, consistent with the absence of a strong local X-ray absorption ($N_{H,loc} \ll 10^{24} \text{ cm}^{-2}$). Further support to the lack of nuclear obscuration for 3C 78 comes from the HST optical data: Chiaberge et al. (1999) detected a pointlike nuclear emission with luminosity $\approx 2 \times 10^{42} \text{ erg s}^{-1}$ in the R band.

The luminosities of the nuclear components are (in the 0.1–2.4 keV energy band) a few $\times 10^{42} \text{ erg s}^{-1}$ for 3C 78 and a few $\times 10^{43} \text{ erg s}^{-1}$ for the other two sources. These values are larger than those found in the sample of Worrall (1997), but consistent with the extrapolation of Worrall’s correlation between the monochromatic X-ray luminosity at 1 keV of the non-thermal component and the core radio power at 5 GHz (see Fig. 8). We note that also in Worrall’s sources there is no evidence of absorption in the non-thermal nuclear components. Since it is likely that the radio galaxies in this sample are distributed at different orientations to the line of sight, we can argue that either the obscuring torus is not present in the FR I radio galaxies, or that the nuclear X-ray emission actually originates from the base of the jets outside the torus, and therefore is not affected by obscuration.

In Fig. 8 we also plot the region typical of LBL (i.e., the revised old class of Radio Selected BL Lacs, see Padovani 1999). We see clearly that our three sources are just in the transition

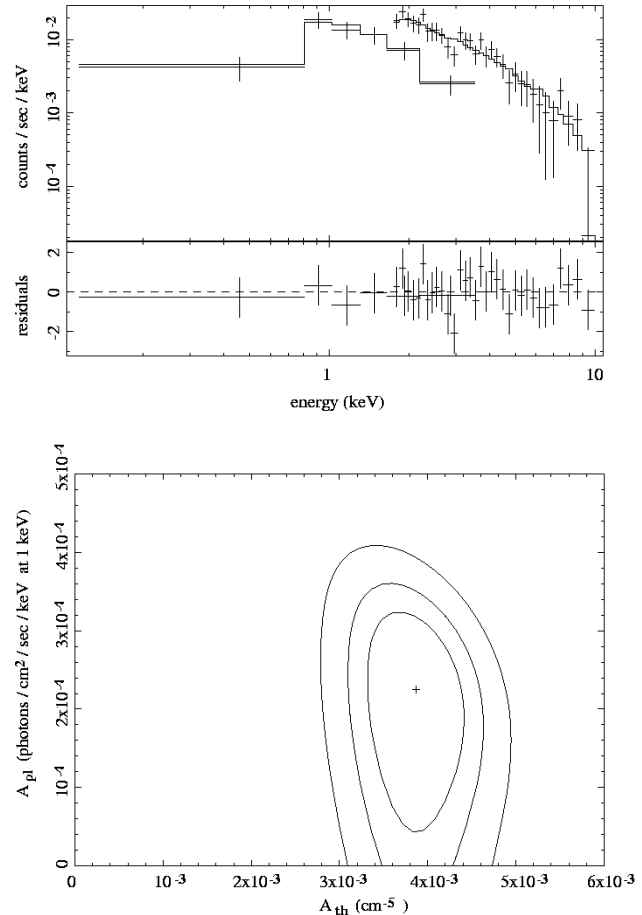


Fig. 7. The same as Fig. 6 for PKS 0620–52, assuming $\alpha = 1.7$ and $N_{H,loc} = 10^{22} \text{ cm}^{-2}$.

region between FR I radio galaxies and BL Lacs. More importantly, we see that the radio - X correlation for the nuclear emission extends also to the LBL region with basically unaffected slope. The main implication of this feature is that the radio - X spectral index $\alpha_{r,X}$ does not significantly change when moving from FR I to BL Lacs objects. If the FR I radio galaxies are just BL Lacs beamed away from the line of sight, the similar values of $\alpha_{r,X}$ for both classes of objects could imply that the detected X-ray non-thermal emission is due to inverse Compton emission (see, e.g., Fossati et al. 1998, and references therein, for a discussion of the main properties of the Spectral Energy Distribution in BL Lacs).

The present data do not allow to draw more stringent conclusions on this point and, more in general, on the unification of FR I radio galaxies and BL Lacs. Besides having a larger sample, it will be crucial to collect detailed information (e.g., with the AXAF and XMM missions) on the spectral properties of the central nucleus in the ≈ 1 –10 keV energy band.

Acknowledgements. The authors wish to thank M. Capalbi, F. Fiore, P. Giommi, M. Guainazzi and S. Molendi for invaluable help in the treatment of the BeppoSAX data. We are indebted to A. Capetti and M. Chiaberge for very helpful discussions and suggestions and to C. Simpson for the radio map of OH-342. This work was partly supported

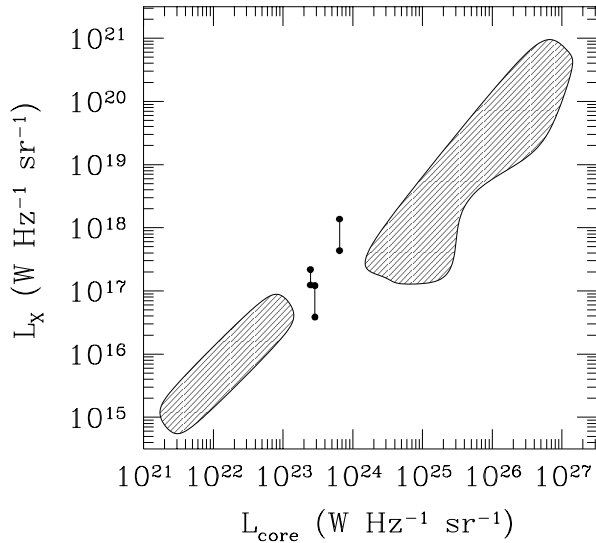


Fig. 8. Plot of the monochromatic X-ray non-thermal luminosity at 1 keV versus the monochromatic core radio luminosity at 5 GHz for our three radio galaxies. For each source the two values L_X (dots connected with a bar) for a flat and steep spectrum are reported, assuming no nuclear absorption for 3C 78 and OH-342, and $N_{H,loc} = 10^{22} \text{ cm}^{-2}$ for PKS 0620–52. In the two shaded areas we report the data (lower left) on FR I from Worrall (1997) and (upper right) on BL Lacs of the LBL type. The latter come from the multi-frequency AGN database of Padovani et al. (1997).

by the Italian Ministry for University and Research (MURST) under grant Cofin98-02-32 and by the Italian Space Agency (ASI).

References

- Abell G.O., Corwin H.G., Olowin R.P., 1989, *ApJS* 70, 1
 Arnaud K.A., Johnstone R.M., Fabian A.C., et al., 1987, *MNRAS* 227, 241
 Baum S.A., Heckman T., Bridle A.H., van Breugel W., Miley G.K., 1988, *ApJS* 68, 643
 Boella G., Butler R.C., Perola G.C., et al., 1997a, *A&AS* 122, 299
 Boella G., Chiappetti L., Conti G., et al., 1997b, *A&AS* 122, 327
 Corbett E.A., Robinson A., Axon D.J., et al., 1996, *MNRAS* 281, 737
 Chiaberge M., Capetti A., Celotti A., 1999, *A&A*, submitted
 De Koff S., Baum S.A., Sparks W.B., et al., 1996, *ApJS* 107, 621
 De Ruiter H.R., Parma P., Fanti C., Fanti R., 1990, *A&A* 227, 351
 Donnelly H.L., Faber S.M., O'Connell R.M., 1990, *ApJ* 354, 52
 Ebeling H., Voges W., Böhringer H., et al., 1996, *MNRAS* 281, 799
 Ekers R.D., Wall J.V., Shaver P.A., et al., 1989, *MNRAS* 236, 737
 Fabbiano G., 1989, *ARA&A* 27, 87
 Fabbiano G., Kim D.-W., Trinchieri G., 1992, *ApJS* 80, 531
 Fanaroff B.L., Riley J.M., 1974, *MNRAS* 167, 31p
 Feretti L., Fanti R., Parma P., et al., 1995, *A&A* 298, 699
 Fiore F., Guainazzi M., Grandi P., 1999, In: *Cookbook for BeppoSAX NFI Spectral Analysis*. BeppoSAX Science Data Center, Version 1.2
 Forman W., Jones C., Tucker W., 1985, *ApJ* 293, 102
 Forman W., Jones C., Tucker W., 1994, *ApJ* 429, 77
 Fossati G., Maraschi L., Celotti A., Comastri A., Ghisellini G., 1998, *MNRAS* 299, 433
 Frontera F., Costa E., Dal Fiume D., et al., 1997, *A&AS* 122, 357
 Gioia I.M., Maccacaro T., Schild R.E., et al., 1984, *ApJ* 283, 495
 Gioia I.M., Luppino G.A., 1994, *ApJS* 94, 583
 Jones P.A., McAdam W.B., 1992, *ApJS* 80, 137
 Kaastra J.S., 1992, Intern. SRON-Leiden Rep., ver. 2.0
 Knapp G.R., Bies W.E., van Gorken J.H., 1990, *AJ* 476, 99
 Manzo G., Giarrusso S., Santangelo A., et al., 1997, *A&AS* 122, 341
 Massaglia S., Trussoni E., Caucino S., et al., 1996, *A&A* 309, 75
 Morganti R., Killeen N.E.B., Tadhunter C.N., 1993, *MNRAS* 263, 1023
 Morganti R., Oosterloo T., Reynolds J.E., Tadhunter C.N., Migenes V., 1997, *MNRAS* 284, 541
 Padovani P., Giommi P., 1996, *MNRAS* 279, 526
 Padovani P., Giommi P., Fiore F., 1997, *Mem. Soc. Astron. Ital.* 68, 147
 Padovani P., 1999, In: Takalo L., Sillanpää A. (eds.) *BL Lac Phenomenon*. ASP Conf. Series, Vol. 159, p. 339
 Parmar A.N., Martin D.D.E., Bavdaz M., et al., 1997, *A&AS* 122, 309
 Ponman T.J., Bourner P.D.J., Ebeling H., 1996a, In: Zimmermann H.U., Trümper J.E., Yorke H. (eds.) *Röntgenstrahlung from the Universe*. MPE rep. 263, 357
 Ponman T.J., Bourner P.D.J., Ebeling H., Böhringer H., 1996b, *MNRAS* 283, 690
 Saikia D.J., Subrahmanya C.R., Patnaik A.R., et al., 1986, *MNRAS* 219, 545
 Sarazin C.L., 1986, *Rev. Mod. Phys.* 58, 1
 Siebert J., Brinkmann W., Morganti R., et al., 1996, *MNRAS* 279, 1331
 Simpson C.J., 1994, Ph.D. Thesis, University of Oxford
 Sparks W.B., Golombek D., Baum S.A., et al., 1995, *ApJ* 450, L55
 Tadhunter C.N., Morganti R., di Serego Alighieri S., Fosbury R.A.E., Danziger I.J., 1993, *MNRAS* 263, 999
 Trussoni E., Massaglia S., Ferrari R., et al., 1997, *A&A* 327, 27
 Ueno S., Koyama K., Nishida M., Yamauchi S., Ward M.J., 1994, *ApJ* 431, L1
 Unger S.W., Booler R.V., Pedlar A., 1984, *MNRAS* 207, 679
 Urry C.M., Padovani P., 1995, *PASP* 107, 803
 Vermeulen R.C., Ogle P.M., Tran H.D., et al., 1995, *ApJ* 452, L5
 Ward M.J., Blanco P.R., Wilson A.S., Nischida M., 1991, *ApJ* 382, 115
 Worrall D.M., Birkinshaw M., 1994, *ApJ* 427, 134
 Worrall D.M., 1997, In: *Relativistic Jets in AGN's*. 20 (astro-ph/9709165)